The Effect of Shear Forces on the Microstructure and Mechanical Properties of Epoxy–Clay Nanocomposites

Tak-keun Oh, Mervat Hassan, Charles Beatty, Hassan El-Shall

Department of Materials Science and Engineering, University of Florida, Gainesville, Florida 32611, USA

Received 1 October 2004; accepted 31 January 2005
DOI 10.1002/app.22134
Published online in Wiley InterScience (www.interscience.wiley.com).

ABSTRACT: The objective of this work is to understand the effect of shear force on the properties of epoxy–clay nanocomposites. The shear force was controlled by changing the revolutions per minute on a mechanical mixer. Differences in the aspect ratio of clay layers and differences of clay particle distribution in the epoxy matrix were caused by shear force. Shear force mechanism on epoxy–clay nanocomposites' intercalation/exfoliation were compared with the other mechanism already suggested. X-ray diffraction, transmission electron microscopy, and scanning electron microscopy were utilized to investigate the degree of exfoliation and morphology. The mechanical and thermal properties were also studied to demonstrate the effect of shear force. This study revealed that appropriate shear force and mixing time on nanocomposite preparation was required to achieve the desired properties. © 2006 Wiley Periodicals, Inc. J Appl Polym Sci 100: 3465–3473, 2006

Key words: epoxy; nanocomposite; shear force; montmorillonite; mechanical property

INTRODUCTION

Polymer nanocomposites containing layer-structured, inorganic nanoparticles (clay) have been extensively researched since the Toyota research group[1–3] reported the greatly improved tensile properties and the enhanced heat distortion temperature of nylon-6 nanocomposites. In general, the dispersion of clay particles in the polymer matrix can result in the formation of three general types of composites: (a) conventional composites; the clay fraction in conventional clay composites plays little or no functional role and acts mainly as a filling agent for economic considerations, (b) intercalated nanocomposites; these are formed when one or a few molecular layers of polymer are inserted into the clay galleries with a fixed interlayer spacing, (c) exfoliated nanocomposites; the individual 10-Å-thick silicate layers are dispersed in the polymer matrix and segregated from one another, and the gallery structures are completely destroyed. Both intercalated and exfoliated nanocomposites offer some special physical and mechanical properties compared to the conventional composites.[4,5]

The in situ polymerization of prepolymers in organoclay galleries has been especially successful for the preparation of exfoliated clay nanocomposites of polyimide,[6,7] unsaturated polyester,[8] polystyrene,[9] polypropylene,[10] and epoxy[4,5,11–16] matrices. Nanoscale layered clays with very high aspect ratio and high strength can play an important role in forming effective polymer nanocomposites due to their intercalation chemistry. Montmorillonite has been particularly important in polymer nanocomposites. Montmorillonite is a crystalline 2 : 1 layered clay mineral in which a central alumina octahedral sheet is sandwiched between two silica tetrahedral sheets.[11]

Epoxy resin is often used in integrated circuit packaging and printed circuit boards, such as in pin grid array packaging, ball grid array packaging, and multiple moduli. To improve the thermal and mechanical properties, inorganic material such as clay is used as an additive in the epoxy resin.[17] Epoxy nanocomposites are also being utilized for a wide range of applications including coating, automotive, and aerospace industries.[16]

Generally, inorganic materials have neither good interaction with organic polymers to achieve good dispersion nor adequate adhesion. Surface modifications have been commonly used to achieve a better interaction of a clay surface to a polymeric matrix. Ion exchange of the Na^+ or Ca^{2+} gallery cations in the pristine minerals by alkylammonium ions is generally chosen to modify the clay interlayer from hydrophilic to hydrophobic and to reduce the physical or electrostatic bonding force of the clay interlayer because it leads to a favorable formation of nanocomposite and to exfoliation of the interlayer of clay.[19,20] Much research was performed regarding the cationic surfactant, such as the effect of chain length and types of surfactant.[15]

Correspondence to: H. El-Shall (erc@erc.ufl.edu).

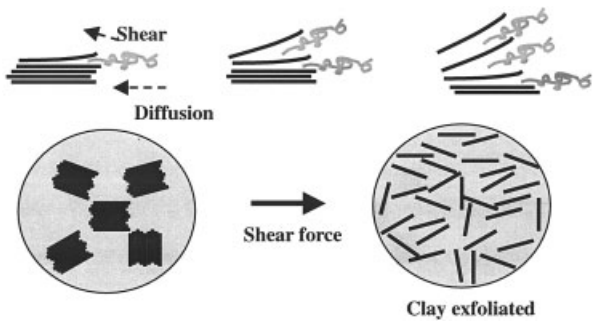

Figure 1 Schematic mechanisms of clay platelets intercalation/exfoliation in the epoxy matrix by shear mixing. Individual platelets peel apart from stack of clay layers.

On the processing side, Vaia et al.[18] have suggested that the degree of exfoliation could be improved through the aid of conventional shear devices. They assumed that the individual plates peel apart through a combination of shear and diffusion of polymer chains in the organoclay gallery, as schematically shown in Figure 1. These authors assume that the platelet on the top or bottom of a stack is able to bend away from others in the stack as the polymer chains seek to wet or make contact with the organoclay surface. As shear force is applied, the solution becomes more viscous with the dispersion of clay particles. At higher clay content, the viscosity increases even further and it is assumed that the extra shear force generated by high viscosity would increase the basal spacing of clay platelets in the epoxy resin. It is therefore suggested that the shear mixing provides good dispersion of clay nanoparticles, including intercalation and exfoliation for the shear force and residence time.[18]

Several investigations of the effect of shear force on properties of thermoplastic nanocomposites have been reported to use shear device such as extruders, mixers, and ultrasonicators.[18] However, thermoset plastics are not suitable for such shear devices. Therefore, the shear force effect onto nanocomposite using thermoset plastics has not been studied extensively. Nevertheless, shear force is an important process parameter for synthesis polymer–clay nanocomposite. In this study, clay–epoxy nanocomposites were prepared using different levels of mixing speed to investigate the effect of shear force, clay loading, and mixing time on intercalation/exfoliation using a mechanical mixer. The shear force was controlled by varying the revolutions per minute (rpm) of the rotor, ranging from 400 to 1000. The thermal, morphological, and mechanical properties were studied with respect to the exfoliation/intercalation.

EXPERIMENTAL

Materials

The clay material is Cloisite 30B from Southern Clay Products. It is a natural montmrillonite organically modified with a methyl tallow bis-2-hydroxyethyl quaternary ammonium. The as-received clay (montmorillonite) particles were disk-like stacks of thin silicate layers, 1 nm thick and ranging from 100 nm to several micrometers in diameter (with an aspect ratio ranging between 200 and 1000). Table I shows the physical properties of Cloisite 30B.[19] The modulus of an individual layer (plates or flake) is 170–180 GPa, and its specific gravity is 1.9–2.1 g/cc. The epoxy resin was the diglycidyl ether of bisphenol A (epoxide equivalent weight = 178 g, EPON 828) and diethytoluenediamine (EPI-CURE W) was used as curing agent, provided by Shell Chemicals.

Preparation of epoxy–clay nanocomposites

The epoxy resin was mixed with a desired amount of organophilic clay (cloisite 30B) in a 2000-mL beaker. A mechanical mixer (Lightnin LabMaster SI Mixer, Model L1U08F, Ireland) that has A310 impeller (86 mm diameter) was used to mix the samples at different speeds (different shear forces). The onium-ion-exchanged clay was dispersed uniformly in epoxy monomer at 80°C for 1 h. Then, a curing agent (diethyltoluenediamine) was added into the epoxy–clay hybrid and mixed thoroughly by the mechanical stirrer. The mixtures were then degassed to remove bubbles using a vacuum oven before they were cast into a mold. The bottom, frame, and top cover of mold were made from aluminum-foil-covered Corning microslides (75 × 50 mm plain, 0.96 to 1.06 nm thickness). The samples were cured in a vacuum oven for at 100 °C for 10 h.

Characterization techniques

The change in the interlayer spacing of clay minerals (montmorillonite and bentonite) was measured using a Philips MRD X'Pert with a rotation anode and CuK_α radiation (λ = 1.5418 Å). The scanning range is from 1.05 to 9.95°. The structure of the clay was investigated at different stages during nanocomposite synthesis. The clay particles were mounted on a sample holder with a large cavity and a smooth surface was obtained by pressing the particles with a glass plate. Analyses

TABLE I
The Physical Properties of Cloisite 30B

Physical properties	Cloisite 30B
Color	Off-white
Density (g/cc)	1.98
d-spacing (d_{001}) (Å)	18.5
Aspect ratio	200–1000
Surface area (m^2/g)	750
Mean particle size (μ)	6

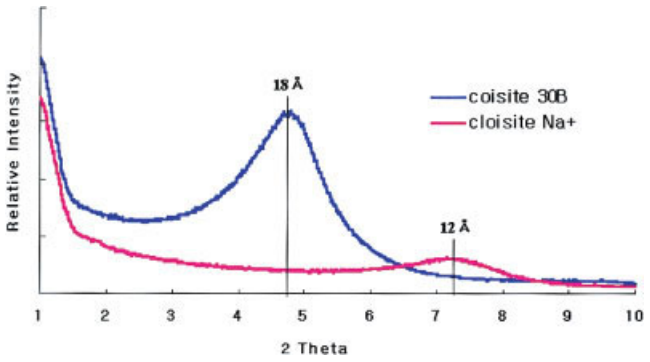

Figure 2 X-ray diffraction patterns of natural montmorillonite and modified montmorillonite. [Color figure can be viewed in the online issue, which is available at www.interscience.wiley.com.]

of organoclay swollen in the epoxy resin or in the curing agent were performed by spreading the mixture on a sample holder. The nanocomposite plates produced during the molding process had a fairly smooth surface.

Fourier transform infrared spectroscopy (Nicolet MAGNA 760) was used to verify the surface modification by the cationic surfactants. The sample was prepared by mixing 90% KBr and 10% clay minerals and then placing it on the disc. Transmittance was used and scans were operated from 1000 to 4000 cm^{-1} and took 124 s to complete.

Differential scanning calorimetry (DSC) tests were carried out on composites using a TA Instruments SDT 2960 simultaneous DSC-TGA analyzer. Samples were heated to 600°C at a scanning rate of 10°C/min under flowing argon. The tensile test was performed on an Endura TEC ELF3200 at a 0.01 mm/s crosshead rate. Samples were prepared to be ~4 mm wide, ~50 mm long, and ~1 mm thick.

The morphology of the nanocomposite was examined by a JSM 6335 field emission scanning electron microscopy (SEM). Fracture surfaces of tensile specimens were coated with carbon to avoid charging and were examined at 5 kV accelerating voltage.

To verify the nanoscale structure, a JEM 2010F transmission electron microscope (TEM) operating at an accelerating voltage of 200 kV was also used. Thin TEM specimens with a thickness of 70 nm were cut from nanocomposite blocks using an ultramicrotome, Leica Ultra Cut.

RESULTS AND DISCUSSION

Natural montmorillonite (cloisite Na^+) has a negatively charged crystalline structure in which a central alumina octahedral sheet is sandwiched between two silica tetrahedral sheets. This natural montmorillonite shows a hydrophilic property. When the cation site is exchanged with cationic surfactants, a methyl, tallow, bis-2-hydroxyethyl, quaternary ammonium, the lattice spacing of clay rises and the hydrophilic nature of montmorillonites changes to an organophilic nature, allowing dispersion in organic solvent. The monomer of epoxy resins readily entered into the gallery of organophilic montmorillonite. X-ray diffraction (XRD) measurements can be used to characterize these gallery spacings if diffraction peaks are observed in the low-angle region: such peaks indicate the d spacing (basal spacing) of ordered-intercalated and ordered-delaminated nanocomposites.

Figure 2 shows different XRD patterns of natural montmorillonite (cloisite Na^+) and cloisite 30B (organically modified montmorillonite). The intergallery spacing was calculated using Bragg's Equation (1),

$$\lambda = 2d \cdot \sin\theta . \quad (1)$$

The interlayer spacing of the cloisite 30B is larger than that of the cloisite Na^+; this is because the cloisite 30B contains a methyl, tallow, bis-2-hydroxyethyl, quaternary ammonium surfactant. Cloisite Na^+ and cloisite 30B (organically modified montmorillonite) show characteristic diffraction peaks at 7.3 and 4.8°, respectively. These 2θ values correspond to interlayer spacing of 12.15 and 18.46 Å, respectively.

When an organomontmorillonite (cloisite 30B) is mixed with epoxy, the peak was shifted to the lower angle at $2\theta = 2.415°$, $d_{(001)} = 36.57$ Å, and the peak of cloisite 30B and diethyltoluenediamine (DETDA) mixture appears at $2\theta = 2.415°$, $d_{(001)} = 35.11$ Å in Figure 3. The result demonstrates that the monomer of epoxy resins or a curing agent was diffused into the galleries, resulting in an increase of the gallery spacing. The peak of organomontmorillonite mixed with epoxy resin or curing agent, which appeared at around 5°, can be explained by the remaining organoclays that

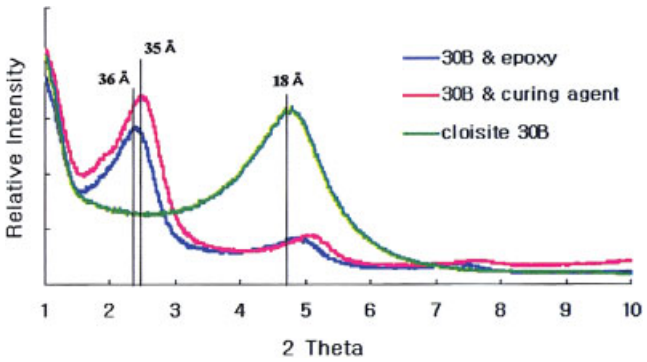

Figure 3 X-ray diffraction peaks of organomontmorillonite (cloisite 30B), epoxy, and cloisite 30B mixture and during agent and cloisite 30B mixture. [Color figure can be viewed in the online issue, which is available at www.interscience.wiley.com.]

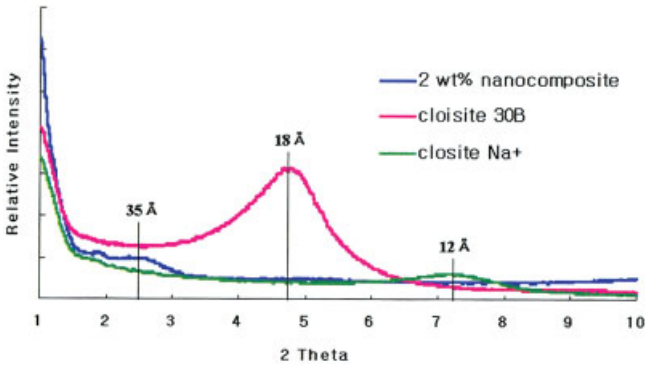

(a) X-ray diffraction Peaks

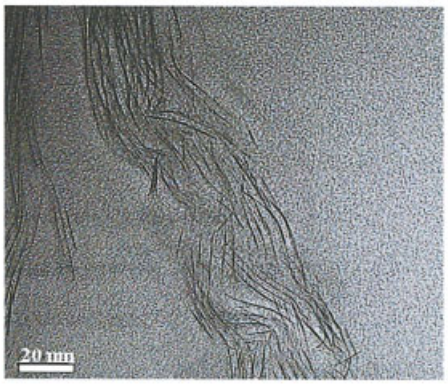

(b) TEM

Figure 4 (a) Compared X-ray diffraction peaks of natural montmorillonite, modified montmorillonite, and 2 wt % cured nanocomposite. (b) TEM image of 2 wt % cured nanocomposite. [Color figure can be viewed in the online issue, which is available at www.interscience.wiley.com.]

the epoxy or curing agent didn't diffuse into the galleries.

The comparison of XRD patterns of natural montmorillonite, modified montmorillonite (cloisite 30B), and a cured nanocomposite with 2 wt % closite 30B loading is shown in Figure 4(a). It is difficult to find a prominent peak in 2 wt % nanocomposite XRD data. This result can be interpreted by the fact that epoxy resin diffused into galleries and formed intercalated or exfoliated nanocomposite. However, if the nanocomposites are disordered, no peaks are also observed in the XRD, due to loss of the structural registry of the layers, the large d-spacing (>10 nm), or both. Thus, XRD of nanocomposites has limitations because a disordered and layered silicate can either be delaminated or intercalated. In such a case TEM combined with XRD will more accurately characterize these materials. Instead of showing a prominent peak in 2 wt % nanocomposite XRD data, the cured nanocomposite with 2 wt % clay loading shows a broad and weak variance around $2\theta = 2.5°$, $d_{(001)} = 35.34$ Å. If this variance can be interpreted as a peak, TEM image may show ~4 nm gallery spacing. Figure 4(b) shows a TEM image of 2 wt % clay nanocomposite, indicating 3–4 nm gallery spacing. Thus, a weak and broad variance can be interpreted as a peak in XRD data, indicating that an intercalated nanocomposite was formed.

Comparing the data in Figures 3 and 4(a), it becomes clear that the cured nanocomposite does not show increased gallery spacing, indicating that no further intercalation occurs during the crosslinking reaction. It can be assumed that the extragallery curing reaction is faster than the intragallery curing reaction. There is no time for a curing agent to go into the galleries. Therefore, the gallery is not expanded and exfoliation does not proceed.

In this study, nanocomposites were prepared using predetermined rpm (shear force) experiments using a mechanical mixer to investigate the effect of shear force. Impeller speed was varied from 400 to 1000 rpm. Tip velocity of this impeller was calculated using eq. (2).

$$v = \omega \cdot r = \text{rpm} \cdot \frac{2\pi}{60} \cdot r \tag{2}$$

$$\frac{F}{A} = \tau = \mu \cdot \omega \,. \tag{3}$$

The velocity profile of the impeller according to the radius at each rpm appears in Figure 5. It can be predicted that the shear force is linearly proportional to the velocity according to eq. (3).

The XRD patterns of different clay contents at fixed tip velocity of the impeller (shear force) are observed in Figure 6. All three X-ray diffraction patterns of cured nanocomposite containing 2, 5, and 7 wt % clay show similar characteristic diffraction peaks of mont-

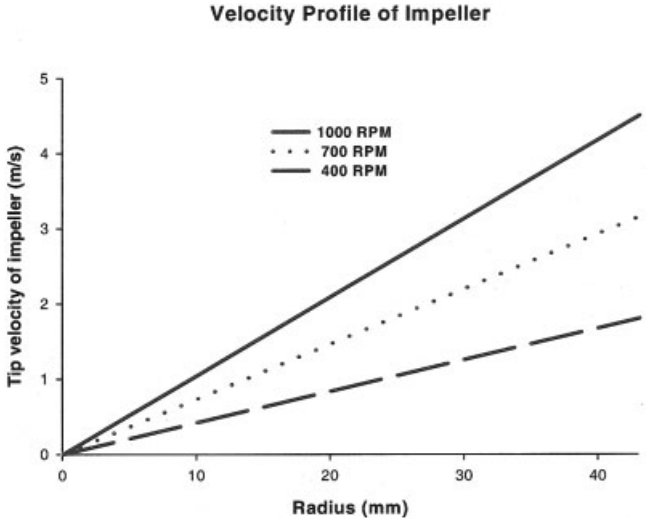

Figure 5 The velocity profile versus impeller radius.

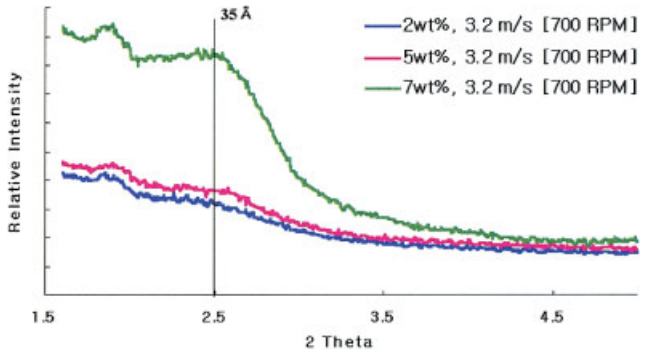

Figure 6 The XRD patterns of epoxy–clay nanocomposite were prepared by different clay loadings. [Color figure can be viewed in the online issue, which is available at www.interscience.wiley.com.]

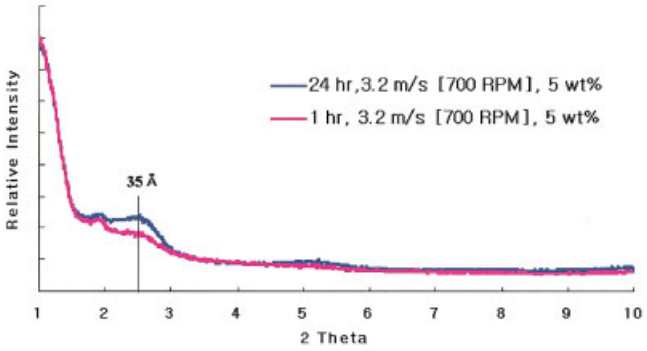

Figure 8 Comparison of XRD patterns on different mixing times. [Color figure can be viewed in the online issue, which is available at www.interscience.wiley.com.]

morillonite at around $2\theta = 1.9°$. The broad and weak peaks appeared at every clay loading nanocomposites at around $2\theta = 2.5°$, $d_{(001)} = 35.34$ Å. This result also shows a sharp increase of intensity with 7 wt % clay loading nanocomposite. It is assumed that high clay loading may require more shear force to break the clay by decreasing the aspect ratio of clay nanoparticles. This broken silicate layer is supported by the increment of the intensity of the XRD peak. The results also reveal that the effect of clay loading amounts on the clay basal spacing is not significant.

XRD patterns for the epoxy resin–clay–DETDA composite with different rpm processed with 7 wt % are shown in Figure 7. Figure 7 also shows a characteristic peak and weak and broad peak intensity change at around $2\theta = 2.5°$, $d_{(001)} = 35.34$ Å. It seems that XRD patterns are not shear force dependent. The peak pattern shows a similar trend at 2 and 5 wt % clay loading amount nanocomposites.

To achieve exfoliated nanocomposites, the galleries continue to expand when the degree of polymerization increases and an exfoliated nanocomposite is formed. If the lattice spacing increases further, the diffraction peak will disappear, indicating an exfoliated nanocomposite. If extragallery polymerization is faster than intragallery polymerization, the epoxy monomer cannot enter between the galleries and basal spacing cannot be increased further, thus forming intercalated nanocomposites. It can be assumed that a large amount of epoxy monomer can enter into the gallery by increasing tip velocity (increasing shear force) and intragallery polymerization can occur at a comparable rate to extragallery polymerization. However, diffraction peaks of an intercalated nanocomposite are observed. This indicates that the shear forces conducted in this research do not affect the intergallery spacin, but rather intergallery spacing is controlled by a chemical reaction factor (crosslinking reaction rate) rather than by mechanical force (shear force).

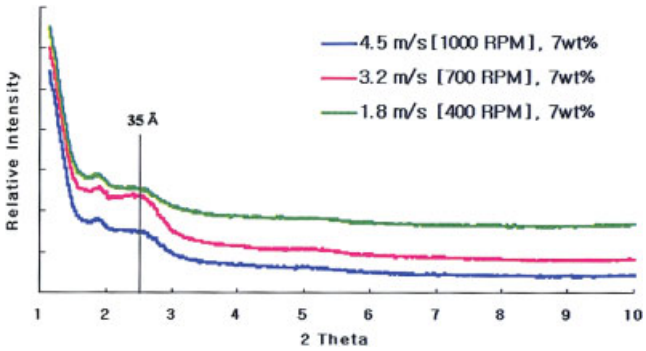

Figure 7 The XRD patterns of epoxy–clay nanocomposite were prepared by different shear force (rpm, tip velocity) at the 7 wt % clay loading. [Color figure can be viewed in the online issue, which is available at www.interscience.wiley.com.]

Figure 8 shows XRD patterns of epoxy–clay nanocomposites at different mixing times. The experiment was performed with 5 wt % clay loading nanocomposits for 24- and 1-h mixing times. No significant difference was observed between 24-h mixing and 1-h mixing conditions, also showing intensity variance around $2\theta = 2.5°$, $d_{(001)} = 35.34$ Å. This increased intensity leads one to believe that more silicate layers are formed by decreasing the aspect ratio of clay. This intensity variance may affect the physical properties of the epoxy–clay nanocomposite. This demonstrates that the mixing conditions could be an important factor while synthesizing the nanocomposite preparation.

The changes seen in XRD can be explained by polymer entering the clay galleries and pushing the platelets apart (i.e., intercalation). As more polymer chains enter the galleries, two possible changes can occur. First, the platelets can loose their ordered, crystalline structure and become disordered with the platelets no longer parallel without pushing the platelets apart. The result is that the XRD peak broadens into the baseline (intercalated disordered). Second, the poly-

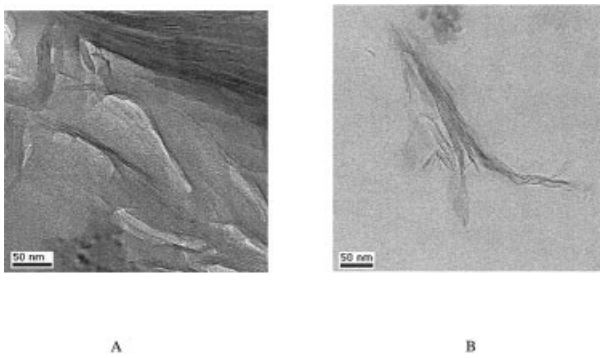

Figure 9 TEM images of nanocomposite at high magnification were (A) prepared by hand mixing and (B) prepared by high shear force (1000 rpm).

mer that enters the galleries pushes the platelets far enough apart that the platelet separation exceeds the sensitivity of XRD (exfoliation). TEM is a better tool to monitor dispersion because the clay platelets can be seen.

Figure 9 shows the TEM image of epoxy–clay nanocomposites with stacks of disordered intercalates at high magnification rather than complete exfoliation. The dark lines are the intersections of silicate layers of 1 nm thickness.

Figure 9(A) shows ~4 nm average distance between clay plates and over 300 nm average length of plates for a 2 wt % hand-mixed processed clay nanocompsite. Figure 9(B) shows ~4 nm average distance between clay plates and 50 nm average length of plates for a 5 wt %, 1000 rpm processed clay nanocomposite. However, X-ray diffraction from these planes does not produce any pronounced peak although the platelets are about 4 nm apart. This could be attributed to either the misalignment or the waviness of clay platelets as seen in Figure 9.

Further intercalation/exfoliation didn't occur according to the clay loading or shear forces, but it seems likely that shear forces break clay particles. The aspect ratio of clay plates is reduced from 200–1000 to 10–50 by increasing shear force. Therefore, it can be suggested that this broken clay particle will be dispersed in the epoxy matrix, providing more surface area.

The morphology of the composite was examined by SEM. Higher shear force induces more evenly distributed clay particles as illustrated in Figure 10(A–D). When clay particles were added to the epoxy matrix, the fractured surface became rougher compared with pristine epoxy [Fig. 10(A)]. The bright spots correspond to the clay aggregates finely dispersed in the material [Fig. 10(B–D)]. As shear forces were increased, smaller clay aggregates appeared but were not evenly distributed. Figure 10(D) shows a rougher fracture surface than Figure 10(B,C). An even distribution of small particles was achieved by prolonging the mixing time.

Evenly distributed clay particles could be as important as achieving an exfoliated nanocomposite. The smaller clay particles can provide more surface area to prevent crack propagation. Thus, it can be concluded that mixing time for nanocomposite preparation is also an important processing parameter and these smaller and evenly distributed clay particles increase mechanical properties.

Mixing clay nanoparticles in an epoxy matrix is expected to improve mechanical properties. Nanoscale clay particles serve a larger surface contact area with the matrix polymer. Thus, it is anticipated that these silicate layers will prohibit crack propagation. Figure 11 shows the stress–strain behaviors of different clay contents fpr hand-mixed (low shear force) nanocomposites under uniaxial tension. As the clay loading amount increases, the tensile strength and the strain to failure decrease. In contrast, the elastic modulus increases with clay content.

In Figure 12(A), the elastic modulus of the nanocomposites increases continuously with increasing clay content. An improvement of the elastic modulus is continuously increased at the beginning and then the rate of improvement decreases. A direct conclusion from these data is that shear force increases the elastic modulus. The broken and evenly distributed particles have more reinforcement in the nanocomposite, which provides blockage to crack propagation.

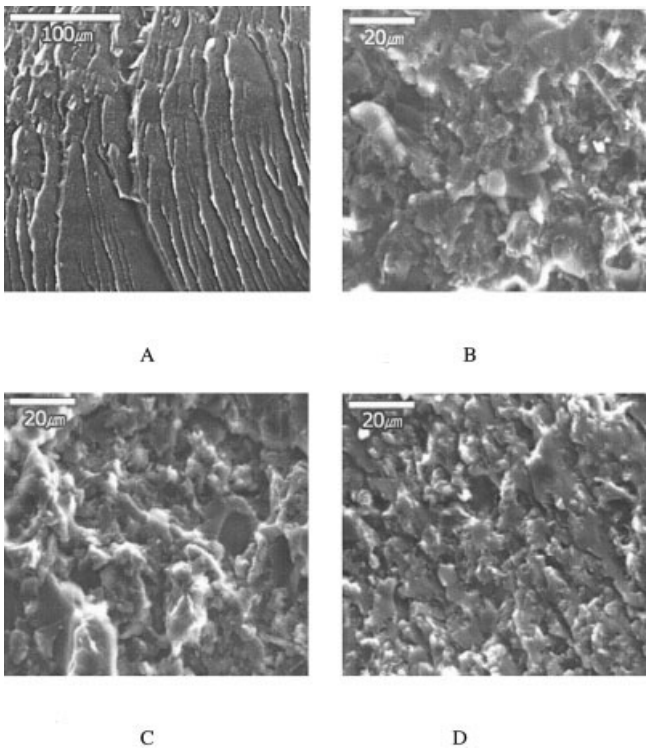

Figure 10 The SEM images of fracture surface at (A) 0 wt %, (B) 400 rpm, 5 wt %, (C) 700 rpm, 5 wt %, and D) 24 h mixing, 700 rpm, 5 wt %.

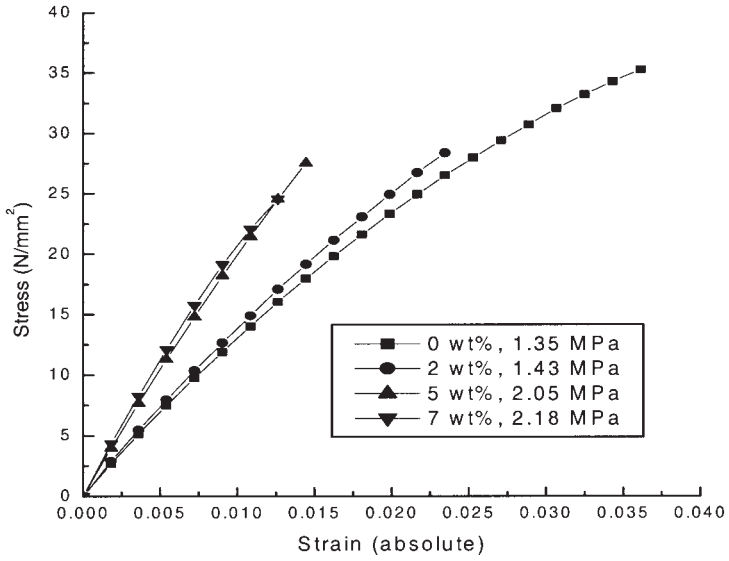

Figure 11 Stress–strain curves of nanocomposites with different wt % clay loading prepared by hand mixing.

The improvement in elastic modulus can be attributed to the exfoliation and good dispersion of nanosized clay particles that restricts the plastic elastic deformation of polymer chains under loading as well as the good interfacial adhesion between the particles and the epoxy matrix. Figure 12(B) shows the variation of elastic modulus with different shear rates at 7 wt % clay content. This result shows no significant change with increasing shear forces. Although shear force makes smaller clay tactoids by decreasing the aspect ratio and increasing the number density, it does not dramatically increase the elastic modulus. The longer mixing of processed nanocomposite has better mechanical properties because of the evenly distributed small clay aggregates [Fig. 10(D)].

The thermal properties of epoxy–clay nanocomposite were investigated by DSC. The glass transition temperature of nanocomposites with different clay contents at 3.2 m/s tip velocity of the impeller (700 rpm) is shown in Table II. This table indicates that T_g (glass transition temperature) increases as clay contents increase. This can be explained by the fact that the movements of amorphous epoxy molecular chains are hindered by finely dispersed clay particles. The thermal properties of epoxy–clay nanocomposites are improved as clay loading increases.

Figure 13 shows that 2 wt % clay loaded samples have lower glass transition temperatures than the no-clay-loaded sample. Also, a lower shear force (1.8 m/s tip velocity) processed sample shows a lower glass transition temperature. This could be attributed to the dispersed particle by increasing shear force, hindering the heat transfer in the epoxy matrix. The glass transition temperatures of 2 wt % clay loaded samples are listed in Table III.

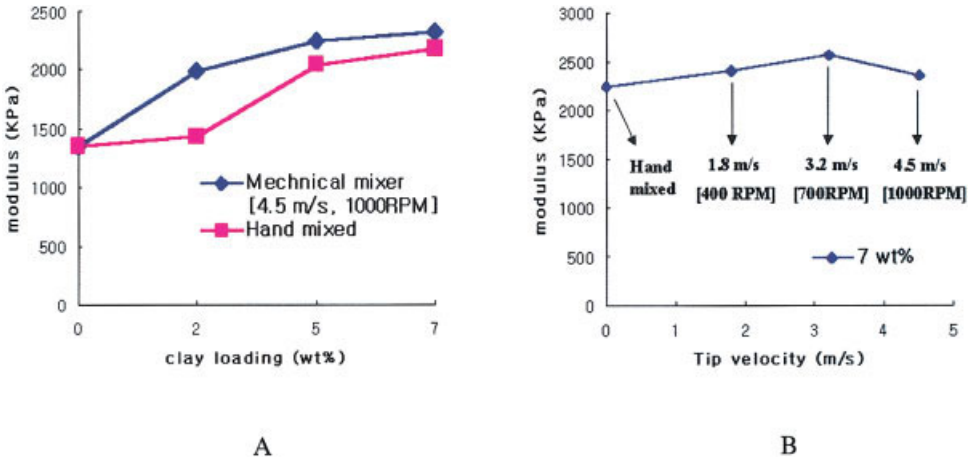

Figure 12 The variation of modulus depends on (A) clay loading and (B) tip velocity of the impeller (shear force). [Color figure can be viewed in the online issue, which is available at www.interscience.wiley.com.]

TABLE II
The T_g Variation of Nanocomposites Prepared with Different Clay Loading

	T_g (glass transition temperature)
No clay	99 ± 3°C
2 wt % clay loading	95.5 ± 3°C
5 wt % clay loading	102.5 ± 2.5°C
7 wt % clay loading	104.5 ± 4°C

TABLE III
The T_g Variation of 2 wt % Clay–Epoxy Nanocomposites with Different Shear Force

	T_g (glass transition temperature)
No clay	99 ± 3°C
400 rpm (1.8 m/s)	94 ± 4°C
700 rpm (3.2 m/s)	95.5 ± 3°C
1000 rpm (4.5 m/s)	97.5 ± 3°C

We now understand that the mechanical and thermal properties of polymer–clay nanocomposites are improved as clay loading increases. Thus, we can expect a higher glass transition temperature as clay loading increases because movement of amorphous epoxy molecular chain is hindered by finely dispersed clay particles. However, DSC results show that the thermal properties of epoxy–organoclay nanocomposites are not consistently improved as clay loading increases. Figure 13 and Table II show that 2 wt % clay loaded samples have lower glass transition temperatures than no-clay-loaded samples. This means that clays in 2 wt % clay loading do not act as fillers. In this case, it may be considered an impurity disrupting the interaction between chains and subsequently reducing the chain–chain interaction forces. This could lead to more chain flexibility or lower glass transition temperature. This is confirmed by the increase in glass transition temperature of the 2 wt % clay loading composite, which was prepared at higher shear forces (Table III). In such cases, the clay has been sheared into a higher number of smaller particles, leading to an increase in the transition temperature. Unlike in 2 wt % clay loading samples, clays at 5 and 7 wt % act as fillers.

The most significant property of epoxy-layered silicate nanocomposite is their high optical transparency. As shown in Figure 14, epoxy–7 wt % clay loading nanocomposite is almost as transparent as pristine epoxy polymer. The curing agent (diethyltoluenediamine) causes a yellow tint in the epoxy–clay nanocomposite. This result suggests that the refractive index of the layered silicate mineral family closely matches that of the organic matrix and the small-size organomontmorillonites are uniformly dispersed in the matrix.

CONCLUSIONS

The intergallery spacing by surface modification can facilitate the entry of epoxy or curing agent molecules into the galleries because the hydrophilic clay surface is changed to an organophilic surface. However, we cannot achieve a completely exfoliated epoxy–clay nanocomposite. This is explained by the fact that the extragallery curing reaction is faster than the intragallery curing reaction. Therefore, no further curing agents or epoxy resins could enter into the galleries and intercalated epoxy–clay nanocomposite is formed. In this regard, there is no effect due to changing loading amount and shear force. The result reveals that the shear force used in this research does not affect the gallery

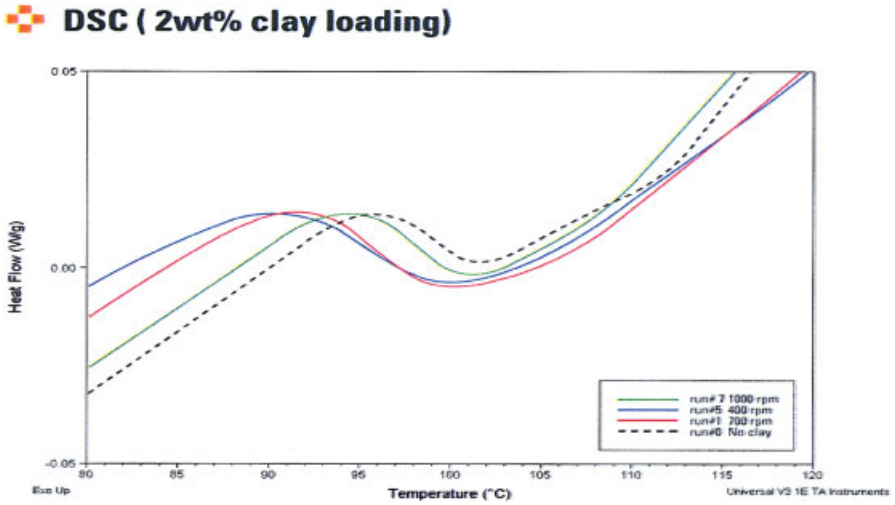

Figure 13 DSC data (2 wt % clay loading with different rpm). [Color figure can be viewed in the online issue, which is available at www.interscience.wiley.com.]

spacing. Therefore, it suggests that the intergallery spacing is affected by the chemical reaction rather than by shear force.

Even though shear force does not lead to an exfoliated nanocomposite, it influences the clay distribution by decreasing the aspect ratio of clay minerals as shown by the TEM analysis revealing the broken silicate layered nanoparticles in the epoxy matrix. Thus, a new model was developed to define the observed result, with modification of Vaia's model as shown in Figure 15.

Vaia et al.[18] assumed that the platelet on the top or bottom of a stack is able to bend away from others in the stack as the polymer chains seek to wet or make contact with the organoclay surface. However, this research shows that when shear forces were increased, the organoclay layers have no flexibility and break up, decreasing the aspect ratio, as shown in Figure 15. As shear stress is applied, the solution becomes more viscous and the high viscosity increases the stress on the whole tactoids of the organoclay. Although individual aluminosilicate layers are flexible, the applied shear force is felted by the whole tactoids. Thus, these tactoids initially break up and individual layers lose their flexibility to peel apart from stack because of decreased aspect ratio.

Tensile modulus was improved by reinforcement with the clay nanoparticles in an epoxy matrix. The hand-mixed nancomposite shows lower tensile modulus than the nanocomposite formed by mechanical mixing. Thus, the shear force does affect the mechanical properties of the epoxy–clay nanocomosite. This may be explained on the basis that small tactoids are dispersed in the epoxy matrix and form high surface area. Thus, this dispersed nanoparticle therefore hinders crack propagation.

Thermal stability is investigated with DSC. As the clay loading amount is increased, the glass transition temperature also is increased. However, at 2 wt % clay loading amount, the glass transition temperature appears below the epoxy glass transition temperature. This means that a small amount of clay loading can act as impurities in the epoxy matrix. A higher amount of clay loading in the nanocomposite shows good transparency, revealing that modified clays are well dispersed in the epoxy matrix.

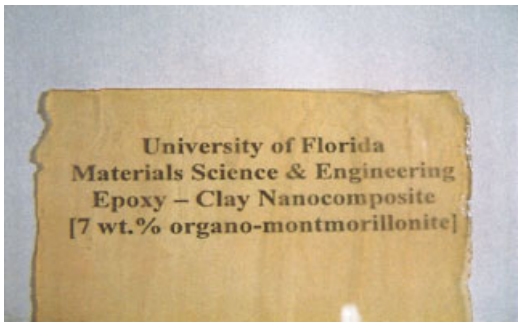

Figure 14 Transparancy of epoxy–clay (7 wt.% clay loading) nanocomposite. [Color figure can be viewed in the online issue, which is available at www.interscience.wiley.com.]

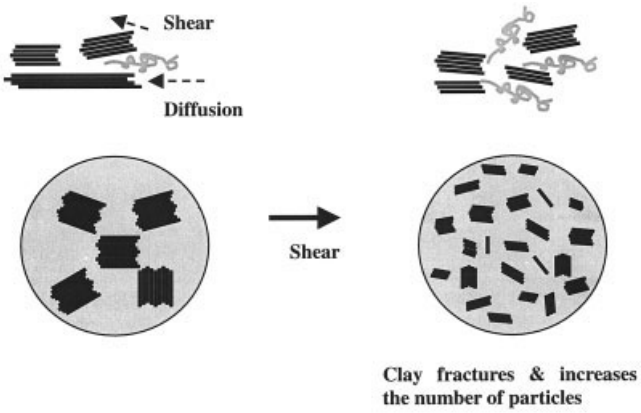

Figure 15 Schematic mechanisms of clay platelets intercalation/exfoliation in the epoxy matrix by shear mixing.

References

1. Usuki, A.; Kawasumi, M.; Kojima, Y.; Okada, A.; Kurauchi, T.; Kamigaito, O. J Mater Res 1993, 8, 1174.
2. Usuki, A.; Kojima, Y.; Kawasumi, M.; Okada, A.; Fukushima, Y.; Kurauchi, T.; Kamigaito, O. J Mater Res 1993, 8, 1179.
3. Kojima, Y.; Usuki, A.; Kawasumi, M.; Okada, A.; Kurauchi, T.; Kamigaito, O. J Polym Sci A Polym Chem 1993, 31, 983.
4. Pinnavaia, T. J.; Beall, G. W. Polymer-Clay Nanocomposite; Wiley: Chichester, 2000.
5. Xu, W.-B.; Bao, S.-P.; He, P.-S. J Appl Polym Sci 2002, 84, 842.
6. Yano, K.; Usuki, A.; Okada, A. J Polym Sci A Polym Chem 1997, 35, 2289.
7. Tyan, H. L.; Liu, Y. C.; Wei, K. H. Chem Mater 1999, 11 1942.
8. Kornmann, X.; Berglund, L. A.; Sterte, J.; Giannelis, E. P. Polym Eng Sci 1998, 38, 1351.
9. Vaia, R. A.; Jandt, K. D.; Kramer, E. J.; Giannelis, E. P. Macromolecules 1995, 28, 8080.
10. Hasegawa, N.; Kawasumi, M.; Kato, M.; Usuki, A.; Okada, A. J Appl Polym Sci 1997, 63, 137.
11. Kornmann, X.; Lindberg, H.; Berglund, L. A. Polymer 2001, 42, 1303.
12. Chin, I.-J.; Thurn-Albrecht, T.; Kim, H.-C.; Russell, T. P.; Wang, J. Polymer 2001, 42, 5947.
13. Salahuddin, N.; Moet, A.; Hiltner, A.; Baer, E. Eur Polym J 2002, 38, 1477.
14. Park. S.-J.; Seo, D.-I.; Lee, J.-R. J Colloid Interface Sci 2002, 251, 160.
15. Chen, K. H.; Yang, S. M. J Appl Polym Sci 2002, 86, 414.
16. Yasmin, A.; Abot, J. L.; Daniel, I. M. Scripta Mater 2003, 49, 81.
17. Bhattacharya, S. K.; Tummala, R. R. Microelectronics J 2001, 32, 11.
18. Vaia, R. A.; Jandt, K. D.; Kramer, E. J. Chem Mater 1996, 8, 2628.
19. Southern Clay Products, Inc. Technical data.
20. Fornes, T. D.; Yoon, P. J.; Keskkula, H.; Paul, D. R. Polymer 2001, 42, 9929.